

## RESEARCH ARTICLE

# NML-mediated rRNA base methylation links ribosomal subunit formation to cell proliferation in a p53-dependent manner

Tsuyoshi Waku<sup>1,\*</sup>, Yuka Nakajima<sup>2,3,†</sup>, Wataru Yokoyama<sup>3</sup>, Naoto Nomura<sup>3</sup>, Koichiro Kako<sup>2,3</sup>, Akira Kobayashi<sup>4</sup>, Toshiyuki Shimizu<sup>1</sup> and Akiyoshi Fukamizu<sup>2,3</sup>

**ABSTRACT**

Ribosomal RNAs (rRNAs) act as scaffolds and ribozymes in ribosomes, and these functions are modulated by post-transcriptional modifications. However, the biological role of base methylation, a well-conserved modification of rRNA, is poorly understood. Here, we demonstrate that a nucleolar factor, nucleomethylin (NML; also known as RRP8), is required for the *N*<sup>1</sup>-methyladenosine (m<sup>1</sup>A) modification in 28S rRNAs of human and mouse cells. NML also contributes to 60S ribosomal subunit formation. Intriguingly, NML depletion increases 60S ribosomal protein L11 (RPL11) levels in the ribosome-free fraction and protein levels of p53 through an RPL11–MDM2 complex, which activates the p53 pathway. Consequently, the growth of NML-depleted cells is suppressed in a p53-dependent manner. These observations reveal a new biological function of rRNA base methylation, which links ribosomal subunit formation to p53-dependent inhibition of cell proliferation in mammalian cells.

**KEY WORDS:** Nucleolar factor, NML, rRNA modification, m<sup>1</sup>A, p53, Cell proliferation

**INTRODUCTION**

Ribosomal RNAs (rRNAs) function as scaffolds for ribosomal proteins and ribozymes for peptide bond formation (Nissen et al., 2000; Steitz and Moore, 2003). Biosynthesis of rRNA comprises transcriptional and post-transcriptional modification of precursor (pre)-rRNAs as well as the processing of pre-rRNAs into mature 28S, 18S and 5.8S rRNAs (Henras et al., 2015). Nucleotide modifications of rRNA regulate the function and stability of ribosomes (Decatur and Fournier, 2002). There are three main types of chemical modifications of rRNA – conversion of uridine to pseudouridine (pseudouridylation); methylation of 2'-hydroxyls (2'-*O*-ribose methylation); and alteration of bases, most of which undergo methylation at different positions (base methylation) (Decatur and Fournier, 2002). Of these modifications, base methylations are the most conserved in terms of their total number and position among living organisms, and are commonly found at approximately ten positions in eukaryotic rRNAs

(Hauenschild et al., 2015; Sharma and Lafontaine, 2015). Base methylation is considered to expand the structural repertoire of RNA, facilitating base stacking by increasing hydrophobicity and adjusting steric hindrance (Ishitani et al., 2008). To date, base methylation of rRNA and the genes responsible for it (Bud23, Rrp8, Nop2, Rcm1, Bmt2, Bmt5 and Bmt6) have been reported in budding yeast (Gigova et al., 2014; Peifer et al., 2013; Sharma et al., 2013; White et al., 2008). A very recent report has shown that yeast and worm homologs of human NSUN5 methylate C2278 in 25S rRNA of *Saccharomyces cerevisiae* and C2381 in 26S rRNA of *Caenorhabditis elegans*; in addition, the reduction in the levels of NSUN5 homologs decreases translational fidelity in yeast and increases the lifespan of *S. cerevisiae*, *C. elegans* and *Drosophila melanogaster* (Schosserer et al., 2015). The human ortholog of yeast Bud23, WBSCR22 (Merm1), has also been shown to mediate *N*<sup>7</sup>-methylation of G1639 and 18S rRNA maturation in cells (Haag et al., 2015); however, little is known about the base methyltransferase of rRNA in mammals.

In all organisms, ribosomes serve as the sole site of biologic protein synthesis, and their biogenesis is strictly regulated. The mammalian ribosome comprises two subunits composed of rRNAs and ribosomal proteins (Anger et al., 2013; Khatter et al., 2015). The small subunit (40S) is formed from a single molecule of rRNA (18S rRNA) and 33 ribosomal proteins (ribosomal proteins of the small ribosomal subunit; RPSs). Conversely, the large subunit (60S) contains three rRNA molecules (5S, 5.8S and 28S) and 47 ribosomal proteins (ribosomal proteins of the large subunit; RPLs). Interestingly, ribosome biogenesis defects are coupled to inhibition of cell proliferation that is mediated by p53 (encoded by *TP53*) (Fumagalli et al., 2009; Sloan et al., 2013; Sulic et al., 2005). p53 functions as a tumor suppressor, and its activation induces apoptosis and cell cycle arrest, resulting in cell growth suppression (Biegging et al., 2014; Brooks and Gu, 2010; Vousden, 2000). Together with these reports, recent studies suggest that quantitative and qualitative changes in ribosomes are associated with numerous physiologic and pathologic events (Barna et al., 2008; Belin et al., 2009, 2010; Figueiredo et al., 2015; Marcel et al., 2013). However, it remains unclear whether and how the base methylation of rRNA regulates ribosomal functions and related biological events in mammals.

Nucleomethylin (NML; also known as RRP8) is a nucleolar protein that binds to dimethyl lysine at position 9 of histone H3 (H3K9me2) in cells and suppresses ribosomal DNA (rDNA) transcription in response to glucose deprivation (Grummt and Ladurner, 2008; Murayama et al., 2008). NML contains the Rossmann-fold methyltransferase-like domain in its C-terminal half, and binds to *S*-adenosyl-L-methionine (SAM), although NML does not exhibit methyltransferase activity toward histones (Murayama et al., 2008). In contrast, the yeast NML homolog Rrp8 has been identified as a gene responsible for the SAM-dependent *N*<sup>1</sup>-methyladenosine (m<sup>1</sup>A) modification in the 25S

<sup>1</sup>Graduate School of Pharmaceutical Sciences, University of Tokyo, Bunkyo-ku, Tokyo 113-0033, Japan. <sup>2</sup>Life Science Center, Tsukuba Advanced Research Alliance (TARA), University of Tsukuba, Tsukuba, Ibaraki 305-8577, Japan.

<sup>3</sup>Graduate School of Life and Environmental Sciences, University of Tsukuba, Tsukuba, Ibaraki 305-8577, Japan. <sup>4</sup>Laboratory for Genetic Code, Graduate School of Life and Medical Sciences, Doshisha University, Kyotanabe, Kyoto 610-0394, Japan.

\*Present address: Laboratory for Genetic Code, Graduate School of Life and Medical Sciences, Doshisha University, Kyotanabe, Kyoto 610-0394, Japan.

†Author for correspondence (nakajima@tara.tsukuba.ac.jp)

 Y.N., 0000-0002-7357-2910

rRNA (Peifer et al., 2013). However, the contribution of NML to m<sup>1</sup>A modification has yet to be elucidated. In this study, using mammalian cells, we reveal that NML is responsible for m<sup>1</sup>A modification of 28S rRNA and contributes to the 60S ribosomal subunit formation, and that NML deficiency inhibits cell proliferation in a p53-dependent manner.

## RESULTS

### NML is required for m<sup>1</sup>A modification in 28S rRNA

In yeast 25S rRNA, two sites with the m<sup>1</sup>A modification have been identified and, along with the neighboring sequences (Peifer et al., 2013), these sites are well conserved among eukaryotes, including in humans and mice (Fig. 1A; Fig. S1; A645 and A2142 of 25S rRNA in *Saccharomyces cerevisiae* correspond to A1309 and A3625 of 28S rRNA in *Homo sapiens*, and A1136 and A3301 of 28S rRNA in *Mus musculus*, respectively). To confirm the interaction between NML and 28S rRNA in human epithelial adenocarcinoma HeLa cells, we performed RNA immunoprecipitation (RIP) experiments using an antibody against NML. In this assay, endogenous NML proteins were precipitated using an antibody against NML. RNAs were then purified from the precipitate, and 28S rRNA levels were quantified by performing quantitative reverse-transcriptase (qRT)-PCR using a specific primer set (Table S1). 28S rRNA was co-immunoprecipitated with NML from the whole cell (Fig. 1B) and nuclear extracts (Fig. 1C), indicating the association of NML with 28S rRNA. By contrast, 5S rRNA was not significantly co-immunoprecipitated with NML (Fig. 1B,C). Next, to investigate the effect of NML on rRNA methylation, we performed a method based on site-specific semi-quantitative RT-PCR using HeLa cells in which NML-knockdown (KD) constructs (shNML#1 and #2) were stably expressed (Fig. 1D, left panel). Methylation levels around A1309, which is methylated by Rrp8 in yeast, were significantly lower in shNML-transfected cells than in control cells expressing shRNAs against green fluorescent protein (shGFP) (Fig. 1D, right panel). However, methylation levels around A3625, which is methylated by Bmt2 in yeast (Sharma et al., 2013), were very low in control cells [rRNA methylation levels around A1309 and A3625 (mean±s.d.) were 19.05±0.47 and 1.32±0.21, respectively. These values were calculated so that the value obtained with the qRT-PCR reaction at the low dNTP concentration was normalized to that obtained at the high dNTP concentration; see Materials and Methods.] and were not markedly changed by knockdown of NML (Fig. S2A). Consistently, methylation levels around A1136, which corresponds to A1309 of 28S rRNA in humans, were reduced in NML-knockout (NML KO) immortalized mouse embryonic fibroblasts (MEFs), compared with in NML wild-type (NML WT) MEFs (Fig. 1E; Fig. S2B). Primer extension analysis was also performed to confirm the modification at A1309 of HeLa cells and A1136 of immortalized MEFs in 28S rRNAs. Strong stop signals at positions A1309 and A1136 were observed in 28S rRNAs of shGFP and NML WT cells (Fig. 1F). By contrast, these stop signals were reduced using 28S rRNAs of NML KD and KO cells. Moreover, the reduction of methylation levels around A1136 was attenuated by the expression of FLAG- and hemagglutinin (HA) FLAG-HA-tagged NML, but not by the expression of control EGFP (Fig. 1G; Fig. S2C). These results indicate that NML is involved in the modifications at A1309 and A1136 in 28S rRNA of human and mouse cells.

To investigate whether NML regulates m<sup>1</sup>A modification of 28S rRNA, we then analyzed the base modifications of RNAs that included a 28S rRNA fragment by performing liquid-chromatography-coupled mass spectrometry (LC-MS/MS). In NML KO and KD cells, the peaks corresponding to m<sup>1</sup>A modification were

reduced compared with those in NML WT and control KD cells (Fig. 2A,B). Moreover, RIP experiments using an antibody against m<sup>1</sup>A revealed that m<sup>1</sup>A modifications around A1136 and A1309 were significantly reduced by NML depletion (Fig. 2C,D). These results indicate that NML is responsible for m<sup>1</sup>A modifications at positions 1309 and 1136 in human and mouse 28S rRNA.

A previous study has revealed that the C-terminal region of NML contains a Rossman-fold methyltransferase-like domain, which interacts with the methyl donor SAM (Murayama et al., 2008) (Fig. 3A). To investigate whether this domain is indispensable for rRNA methylation, we performed a site-specific semi-quantitative RT-PCR-based method using the immortalized MEFs that stably expressed FLAG-HA-tagged wild-type NML (NML-wt) or mutated NML constructs (NML-mt1 or NML-mt2) that lack the ability to bind to SAM (Murayama et al., 2008) (Fig. 3A,B). Expression of NML-wt increased rRNA methylation levels around A1136 in NML KO cells (Fig. 3C). Conversely, no significant enhancement of rRNA methylation was induced by expression of control EGFP, NML-mt1 or NML-mt2 in NML KO cells. These results suggest that NML regulates m<sup>1</sup>A modification in 28S rRNA through its methyltransferase-like domain.

### NML contributes to the formation of the 60S ribosomal subunit

Modifications of rRNA contribute to ribosomal subunit formation and association (Decatur and Fournier, 2002; Polikanov et al., 2015). To investigate the effect of knockdown of NML on the interaction between ribosomal subunits, we used bimolecular fluorescence complementation (BiFC) to visualize ribosomal subunit joining (Al-Jubran et al., 2013). The 40S ribosomal protein S18 (RPS18) and 60S ribosomal protein L11 (RPL11), which are adjacent to each other on the surface of each subunit, were tagged with the N- and C-terminal halves of the yellow fluorescent protein Venus, respectively (yielding S18-VN and L11-VC; Fig. 4A). Subunit interaction was detected as Venus signal (hereafter referred to as BiFC signal; see Materials and Methods). We validated this assay using fluorescence-activated cell sorting (FACS) and confirmed that the BiFC signal was only detected when S18-VN and L11-VC were co-transfected (Fig. 4B). Moreover, the BiFC signal was dramatically reduced when cells were treated with puromycin, an aminoacyl-tRNA-like molecule that causes 80S dissociation (Al-Jubran et al., 2013; Blobel and Sabatini, 1971) (Fig. 4B–D). These results suggest that the BiFC signal derived from S18-VN and L11-VC expression is a consequence of subunit interaction. Knockdown of NML increased the population of cells that emitted a low BiFC signal and decreased the proportion of cells that emitted a high BiFC signal (Fig. 4C). The median BiFC signals were also decreased by knockdown of NML (Fig. 4D). We then performed sucrose density gradient centrifugation in the presence of EDTA, which dissociates the 80S complex into the 40S and 60S subunits (Peifer et al., 2013); the cell lysates were centrifuged and fractionated, and the ribosomal subunit ratio was quantified by measuring the 18S and 28S rRNA levels in each fraction (Fig. 5A). The ratio of 18S rRNA:28S rRNA (amount of 18S rRNA divided by the amount of 28S rRNA) in shNML cells was significantly higher than that of shGFP cells (Fig. 5B). Notably, in these cell lines, 18S and 28S rRNAs were distributed to similar extents in fractions 4–8 and 9–15, respectively (Fig. 5A). Considering that this assay separates cellular organelles, including ribosomal subunits, depending on their individual densities (mass/volume), these results indicate that knockdown of NML results in fewer 60S subunits, rather than the formation of abnormal subunits.

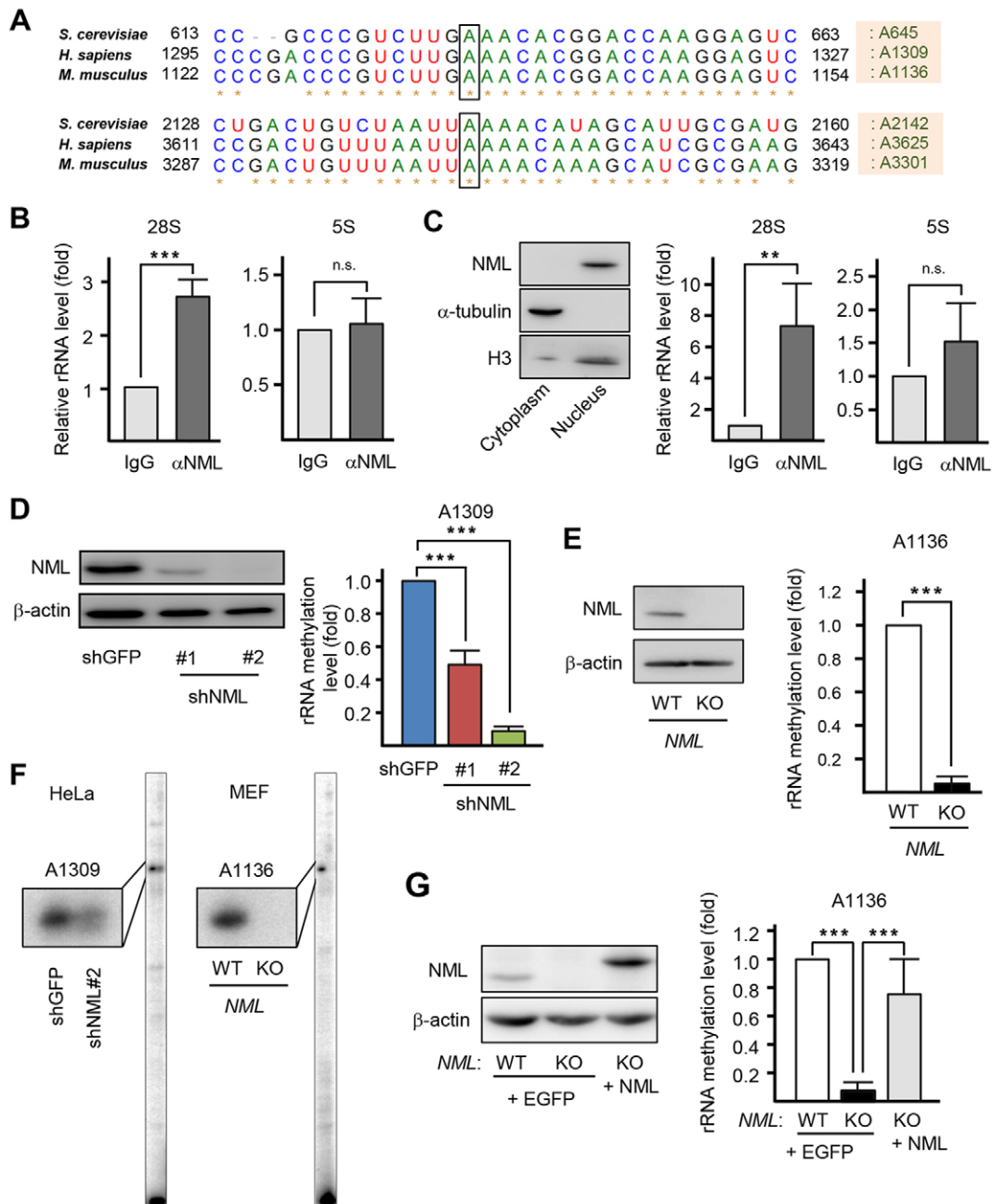


**Fig. 1. NML is required for modification in 28S rRNA.** (A) Multiple sequence alignment of the regions neighboring two positions of  $N^1$ -methyladenosine ( $m^1A$ ; A645 and A2142 in squares) of 25S rRNA (613–663 and 2128–2160) in *Saccharomyces cerevisiae*, of 28S rRNA (1295–1327 and 3611–3643) in *Homo sapiens* and of 28S rRNA (1122–1154 and 3287–3319) in *Mus musculus*. Conserved nucleotides are marked with asterisks. (B,C) Interaction between rRNA and NML in whole-cell extracts (B) and nuclear extracts (C) of HeLa cells. The binding of NML to 28S or 5S rRNAs was validated with RIP using an antibody against NML ( $\alpha$ NML). An unconjugated affinity purified immunoglobulin (IgG) from mouse was used as a control. In the left panel in C, protein levels of NML in the indicated fractions were determined using western blot.  $\alpha$ -tubulin and histone H3 (H3) were also used as cytoplasmic and nuclear markers, respectively. (D) Methylation levels at a region of 28S rRNA, including A1309, in HeLa cells expressing shRNAs targeting GFP (shGFP) or NML shNML#1 or shNML#2 were analyzed by performing qRT-PCR (right panel). shGFP was used as a control shRNA. Protein levels of NML in the indicated cells were determined using western blot (left panel). (E) Methylation levels were analyzed by performing qRT-PCR (right panel) at a region of 28S rRNA, including A1136, in NML wild-type (WT) or knockout (KO) immortalized MEFs. Protein levels of NML in the indicated cells were determined using western blot (left panel). (F) Modification state at A1309 of human 28S rRNA in shGFP- or shNML#2-expressing HeLa cells and at A1136 of mouse 28S rRNA in NML WT or KO immortalized MEFs, analyzed by using primer extension tests. (G) Expression of FLAG and HA (FLAG–HA)-tagged NML recovered the methylation levels around A1136 of 28S rRNA in NML WT or KO immortalized MEFs, demonstrated using western blot (left panel) and qRT-PCR (right panel). All values are presented as mean  $\pm$  s.d. of three independent experiments. \*\* $P < 0.01$ ; \*\*\* $P < 0.005$ ; n.s., not significant (bootstrap and permutation tests) in B–E, G).

Next, we tested whether NML depletion alters bulk protein translation by incorporating  $^{35}\text{S}$ -labeled methionine ( $^{35}\text{S}$ -Met) into proteins. Pretreatment with protein synthesis inhibitor cycloheximide (CHX) fully blocked amino acid incorporation into newly synthesized

proteins (Fig. 5C). In NML KD cells, the rates of  $^{35}\text{S}$ -Met incorporation were not markedly different from those in control cells. Overall, these results suggest that NML is involved in the formation of 60S ribosomal subunits without affecting bulk protein synthesis.

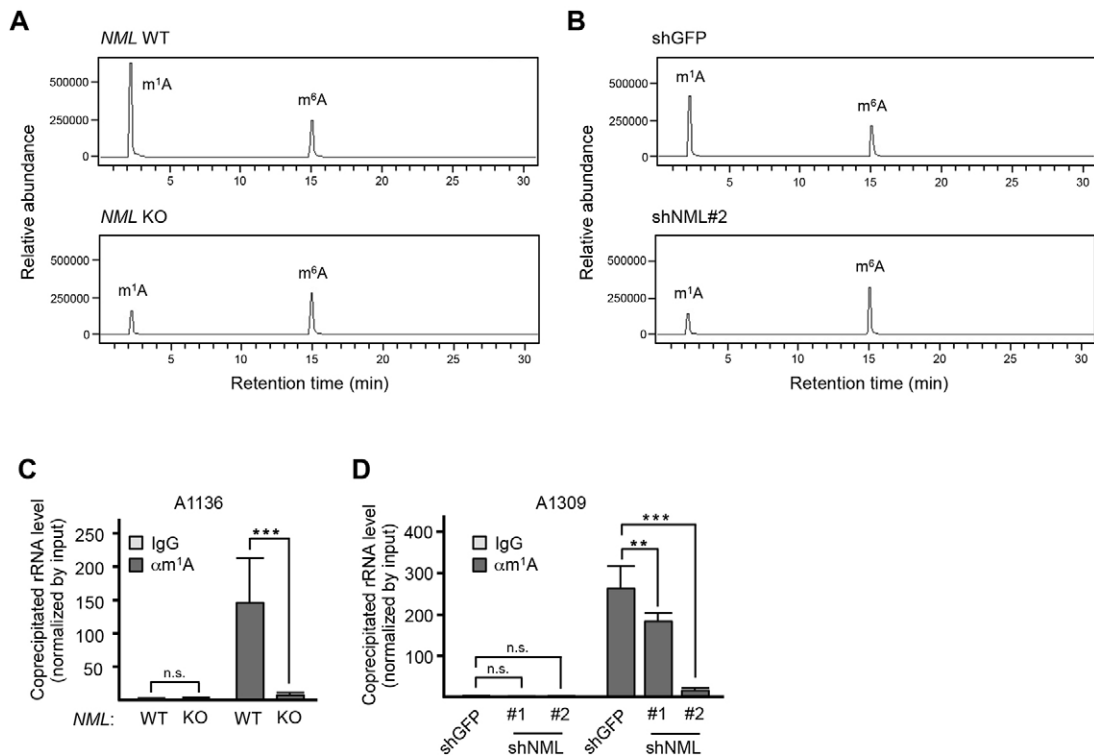


**Fig. 2. NML is involved in m<sup>1</sup>A modification in 28S rRNA.** (A,B) The amount of 28S rRNA m<sup>1</sup>A modified in *NML* WT or KO immortalized MEFs (A) and shGFP or shNML#2 HeLa cells (B) was analyzed by performing LC-MS/MS. (C,D) m<sup>1</sup>A levels around A1136 in 28S rRNA of *NML* WT or KO immortalized MEFs (C) and around A1309 in 28S rRNA of shGFP- or shNML-expressing HeLa cells (D) analyzed by RIP using an antibody against m<sup>1</sup>A ( $\alpha$ m<sup>1</sup>A). An unconjugated affinity purified IgG from mouse was used as a control. Values are presented as mean $\pm$ s.d. of three independent experiments. \*\*\* $P$ <0.005; n.s., not significant (Student's  $t$ -test) in C. \*\* $P$ <0.01; \*\*\* $P$ <0.005; n.s., not significant (one-way ANOVA followed by Tukey's test) in D.

Previous reports have shown that NML inhibits rDNA transcription in human cells under glucose deprivation, but not under conditions with 1 g/l glucose (Murayama et al., 2008; Yang et al., 2013) (Fig. S2D). Moreover, it has been reported that the depletion of certain factors involved in ribosome biogenesis inhibits rDNA transcription and/or pre-rRNA processing (Bousquet-Antonelli et al., 2000). We investigated the effect of knockdown of NML on rDNA transcription and processing under conditions with 4.5 g/l glucose used in this study. In shNML-expressing HeLa cells, mature and pre-rRNA levels were unchanged in comparison with those in control cells (Fig. S2D). Furthermore, analysis of pre-rRNA processing using metabolic labeling with <sup>32</sup>P-orthophosphate

showed that there was no substantial change in the distribution patterns on gels of pre-rRNA (47S and 45S, and 32S) and mature rRNA (28S and 18S) between shNML- and shGFP-expressing HeLa cells (Fig. S2E). These results indicate that NML affects rRNA base methylation without altering rDNA transcription and pre-rRNA processing under normal glucose conditions.

### NML depletion induces activation of the p53 pathway through RPL11

Location of ribosomal proteins outside of the ribosome increases when ribosomal biogenesis is perturbed by nucleolar stress (Miliani de Marval and Zhang, 2011; Zhang and Lu, 2009). Several

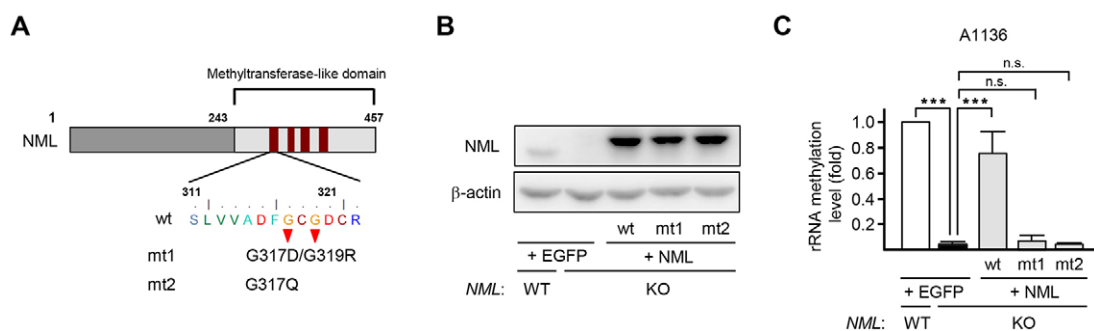


**Fig. 3. NML regulates 28S rRNA methylation through its Rossmann-fold methyltransferase-like domain.** (A) Schematic representation of wild-type (wt) NML and point mutants in the Rossmann-fold methyltransferase-like domain (mt1 and mt2). Conserved motifs in the SAM-methyltransferase are shown in red bars. (B) Protein levels of NML in *NML* WT or KO immortalized MEFs expressing EGFP as a control. Expression of wild-type or mutated (mt1 or mt2) FLAG-HA-tagged NML was analyzed using western blot. (C) Methylation levels around A1136 of 28S rRNA in *NML*-KO immortalized MEFs, demonstrated by qRT-PCR analysis. Values are presented as mean $\pm$ s.d. of three independent experiments. \*\*\* $P$ <0.005; n.s., not significant (bootstrap and permutation tests).

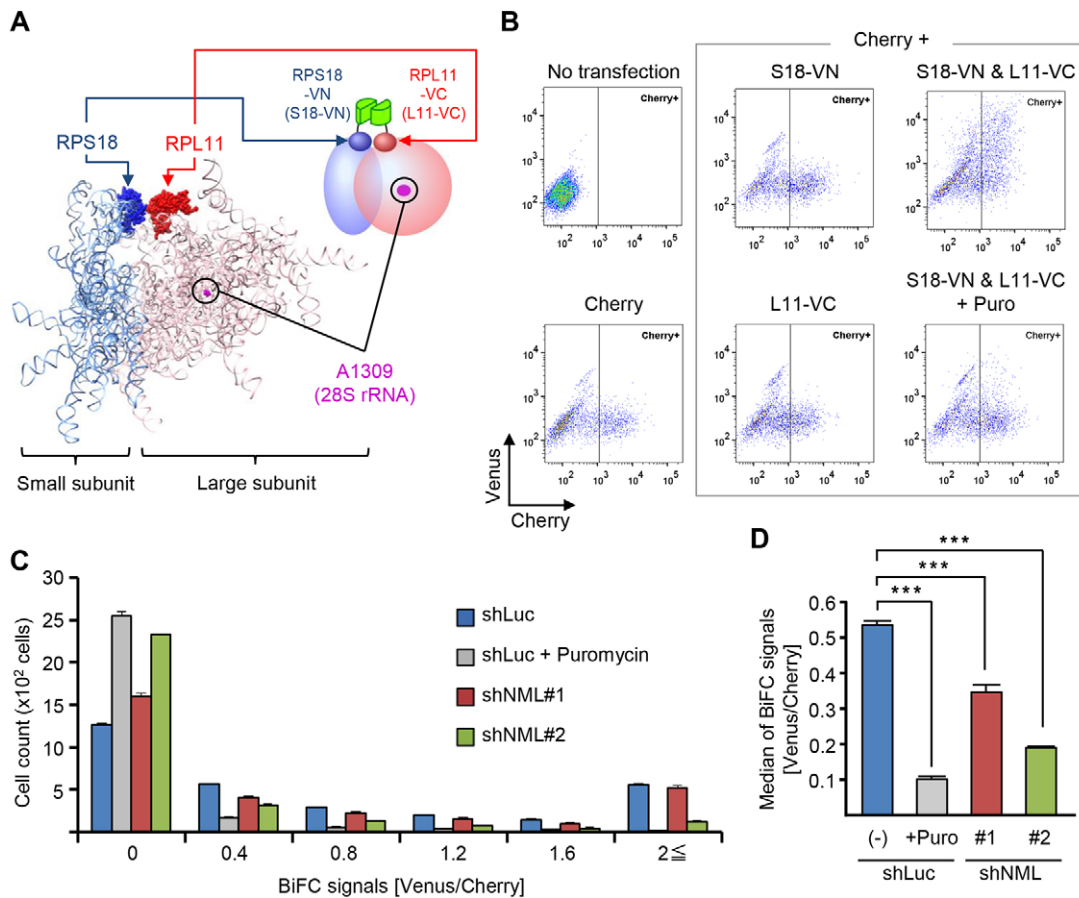


**Fig. 4. The effect of knockdown of NML on the interaction between ribosomal subunits.** (A) Crystal structure of the human ribosome (Protein DataBank ID, 4V6X; Khatter et al., 2015). RPS18 and RPL11 and A1309 are highlighted in different colors. The BiFC model of the ribosome is also schematically represented. In this model, RPS18 and RPL11 are tagged with the N- and C-terminal parts of Venus, respectively (S18-VN and L11-VC). (B–D) The interaction between ribosomal subunits in HeLa cells expressing shRNA targeting luciferase (shLuc) or *NML* (shNML#1 or #2) was analyzed by using BiFC following FACS analysis. shLuc was used as a control shRNA. S18-VN and/or L11-VC were co-expressed in cells with mCherry as a transfection control marker, and treated with or without puromycin (puro). Venus and mCherry emissions (BiFC signals) for shLuc-expressing HeLa cells in the conditions indicated are plotted in B. The distribution and median of the BiFC signals are shown in C and D, respectively. Values are presented as mean±s.d. of three independent experiments. \*\*\* $P$ <0.005 (one-way analysis of variance followed by Tukey's test).

ribosomal proteins, including RPL11, bind to MDM2 and inhibit the E3 ubiquitin ligase function of MDM2 toward p53, leading to p53 stabilization and activation (Deisenroth and Zhang, 2010; Lohrum et al., 2003; Zhang et al., 2003). To investigate whether NML is involved in p53 activation through ribosomal proteins (Fig. 6A), we analyzed the levels of RPL11 protein in the ribosome-free fraction by performing sucrose density gradient centrifugation in the absence of EDTA. The amount of ribosome-free RPL11 was increased in shNML cells (Fig. 6B; Fig. S3A), indicating elevated RPL11 accumulation outside of the ribosome. Moreover, co-immunoprecipitation experiments showed that the interaction between RPL11 and MDM2 was increased in shNML cells (Fig. 6C). p53 activity in the immortalized MEFs and HeLa cells is inhibited by SV40 large T-antigen and by E6 protein from oncogenic HPV type 16, respectively (Hoppe-Seyler and Butz, 1993; Kierstead and Tevethia, 1993). Thus, we used human colon carcinoma HCT116 *tp53* wild-type ( $p53^{+/+}$ ) and null ( $p53^{-/-}$ ) cells, and investigated the possibility that NML depletion induces p53 activation through RPL11. In  $p53^{+/+}$  cells, knockdown of NML increased p53 protein levels, and this p53 accumulation was abrogated by knockdown of RPL11 (Fig. 6D). The expression of p53 target genes was induced by knockdown of NML in  $p53^{+/+}$  cells, but not in  $p53^{-/-}$  cells, at both the mRNA and protein level

(Fig. 7). The activation of p53 target genes induced by NML depletion was also observed in normal MEFs, but not in the immortalized MEFs (Fig. S3B). Taken together, these results indicate that NML knockdown increases the RPL11–MDM2 interaction and induces p53 activation.

#### NML regulates cell proliferation in a p53-dependent manner

p53 contributes to the regulation of cell proliferation by inducing apoptosis and cell cycle arrest, or by inhibiting protein synthesis (Biegging et al., 2014; Brooks and Gu, 2010; Tilleray et al., 2006; Vousden, 2000). We investigated the effect of NML on these p53-dependent cellular events. A terminal deoxynucleotidyl transferase dUTP nick-end labeling (TUNEL) assay showed that the percentage of TUNEL-positive cells was significantly increased by NML knockdown in  $p53^{+/+}$  cells, whereas this was not the case in  $p53^{-/-}$  cells (Fig. 8A; Fig. S4A). Moreover, cell cycle analysis revealed that NML knockdown decreased the proportion of S-phase cells and increased the proportion of G2- and M- (G2/M) phase cells in a p53-dependent manner 3 days after transfection with small interfering (si)RNAs (Fig. 8B; Fig. S4B). The rates of <sup>35</sup>S-Met incorporation into synthesized proteins were reduced by NML knockdown in  $p53^{+/+}$  cells (Fig. 8C). By contrast, in  $p53^{-/-}$  cells, the rates of incorporation of the labeled amino acid were not significantly

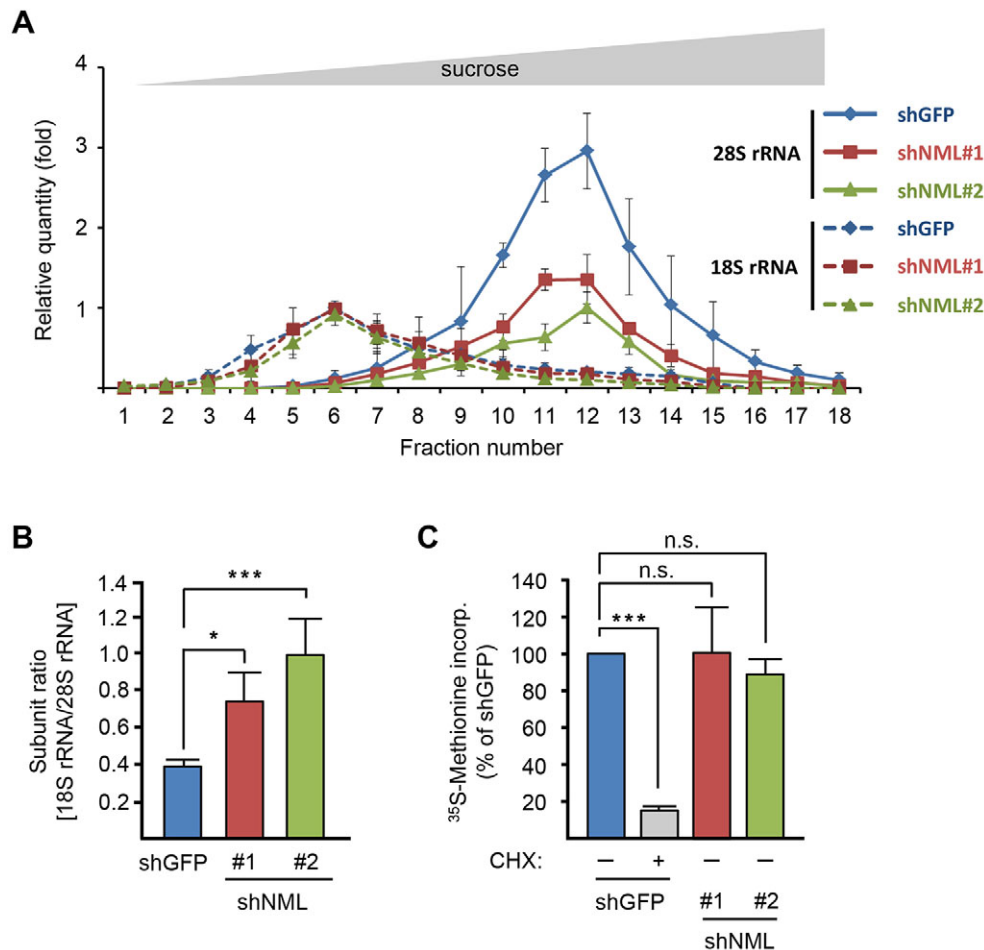


**Fig. 5. NML is involved in the formation of 60S ribosomal subunit.**

(A,B) Ribosomal subunit formation in shGFP-, or shNML#1- or shNML#2-expressing HeLa cells were analyzed by performing sucrose density gradient centrifugation following qRT-PCR. 18S and 28S rRNA levels in each fraction were normalized against those in an input (A). The ratios between the total amounts of 18S and 28S rRNAs are shown as subunit ratios for the cells indicated (B). (C) The total protein synthesis rate in the cells indicated was measured based on <sup>35</sup>S-methionine incorporation (incorp.) into newly synthesized proteins. Cycloheximide (CHX) was used as a positive control. All values are presented as mean±s.d. of three independent experiments. \**P*<0.05; \*\*\**P*<0.005; n.s., not significant (one-way ANOVA followed by Tukey's test) in B. \*\*\**P*<0.005; n.s., not significant (bootstrap and permutation tests) in C.

changed by NML knockdown. Consistent with these results, cell proliferation was suppressed by NML knockdown in a p53-dependent manner (Fig. 8D). NML knockdown also significantly reduced methylation levels around A1309, as well as interactions between ribosomal subunits in both *p53*<sup>+/+</sup> and *p53*<sup>-/-</sup> cells (Fig. 8E,F). Overall, our findings suggest that NML is involved in large ribosomal subunit formation through m<sup>1</sup>A modification of 28S rRNA, thereby regulating cell proliferation through the p53 pathway.

## DISCUSSION

We showed that the nucleolar protein NML regulates m<sup>1</sup>A modification of 28S rRNA in a SAM-binding-domain-dependent manner (Figs 1–3). Additionally, NML depletion decreases 60S subunit formation (Fig. 5A,B). Intriguingly, we observed that NML depletion enhances RPL11–MDM2 interactions and increases levels of p53 protein, thereby activating the p53 pathway (Figs 6 and 7). Consequently, the proliferation of NML-depleted cells is suppressed by p53-dependent apoptosis, cell cycle arrest and protein synthesis inhibition (Fig. 8A–D). Therefore, our results suggest that NML is involved in the m<sup>1</sup>A modification of 28S rRNA and that a deficiency in NML inhibits cell proliferation in a p53-dependent manner.

NML was first identified as an H3K9me2-binding protein that forms a complex with SIRT1 and SUV39H1 to suppress rDNA transcription under glucose starvation (Murayama et al., 2008). Our data raise the question of how the molecular function of NML switches from an epigenetic suppressor to a base methyltransferase. Interestingly, it has been recently reported that NML binds directly to rRNA under normal glucose conditions

(Yang et al., 2013). Conversely, glucose deprivation inhibits the interaction between NML and rRNA, thereby enhancing the recruitment of SIRT1 to NML. Indeed, we confirmed that, at a glucose concentration of 4.5 g/l, NML interacts with 28S rRNA in HeLa cells (Fig. 1B,C) and that NML depletion does not change the level of rDNA transcription (Fig. S2D). These results suggest that NML functions as a methyltransferase for rRNA under normal glucose conditions, whereas it functions as a suppressor of rDNA transcription under glucose deprivation. Thus, NML might modulate distinct steps of ribosome biogenesis, involving rDNA transcription and rRNA methylation, in response to environmental changes.

Of the rRNA modifications, 2'-*O*-ribose methylation, which affects not only ribosome biogenesis but also ribosomal functions, including translational efficiency and fidelity (Decatur and Fournier, 2002), is one of the best characterized. Furthermore, fibrillarin (FBL) has been identified as a 2'-*O*-ribose methyltransferase (Decatur and Fournier, 2003; Lin et al., 2011). Recently, it has been reported that p53 directly represses *FBL* transcription and decreases the 2'-*O*-ribose methylation of rRNAs, impairing the translational function of ribosomes (Marcel et al., 2013). Furthermore, FBL overexpression facilitates tumorigenesis and is associated with poor survival of cancer-affected individuals, implying that rRNA modification plays a crucial role in cancer development. Indeed, levels of m<sup>1</sup>A-modified nucleosides are elevated in the urine of individuals with cancer (Itoh et al., 1992, 1988). Our results suggest that the NML-dependent m<sup>1</sup>A modification of rRNA could influence cancer development through the p53 pathway. Therefore, potential roles of NML-dependent modifications of rRNA in cancer development should be explored.

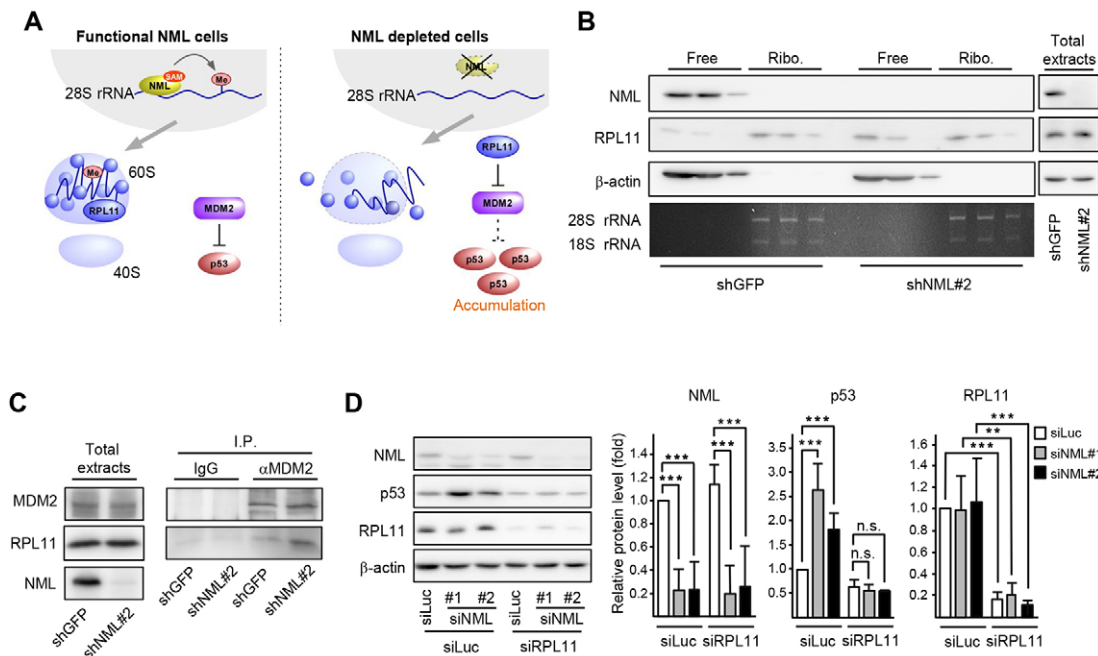


**Fig. 6. NML depletion increases p53 protein levels through RPL11.** (A) Schematic model of NML-dependent p53 accumulation through RPL11. In functional NML cells, p53 is degraded by MDM2 (left pathway). Depletion of NML increases ribosome-free RPL11, which enhances the interaction of RPL11 with MDM2 and induces p53 accumulation (right pathway). (B) Protein levels of RPL11 in the ribosome-free (free) or ribosomal (Ribo.) fraction of shGFP- or shNML#2-expressing HeLa cells were analyzed by performing sucrose gradient centrifugation followed by western blotting (top three rows). 18S and 28S rRNAs are shown as references for ribosome sedimentation (bottom row). (C) Interaction between RPL11 and MDM2 in shGFP- or shNML#2-expressing HeLa cells was analyzed using immunoprecipitation (I.P.) with an antibody against MDM2 and western blotting. An unconjugated affinity purified IgG from mouse was used as a control for immunoprecipitation. (D) Protein levels of p53 in HCT116  $p53^{+/+}$  cells that had been treated with siRNA targeting luciferase (siLuc) or NML (siNML#1 or siNML#2) and/or RPL11 (siRPL11). Two days after siRNA transfection, the levels of the indicated proteins were analyzed using western blot. Representative western blot data are shown on the left. Graphs are expressed as the fold change relative to the indicated protein levels in siLuc-transfected HCT116  $p53^{+/+}$  cells. Values are presented as mean  $\pm$  s.d. of three independent experiments. \*\* $P < 0.01$ ; \*\*\* $P < 0.005$ ; n.s., not significant (bootstrap and permutation tests).

## MATERIALS AND METHODS

### Cell culture

HeLa cells were provided by the RIKEN Catalysis Research Center through the National Bio-Resource Project of the Ministry of Education, Culture, Sports, Science and Technology, Japan. Dr Akiko Murayama (University of Tsukuba, Tsukuba, Japan) gifted SV40 large-T-antigen-immortalized NML WT and KO MEFs, which were generated from C57BL/6J background wild-type and NML-KO mice (Oie et al., 2014), respectively. HCT116  $p53^{+/+}$  and  $p53^{-/-}$  cells were kindly provided by Dr Bert Vogelstein (John Hopkins University, Baltimore, MD) (Bunz et al., 1998). All animal experiments were approved and performed in accordance with the guidelines for the care and use of laboratory animals at University of Tsukuba. For MEF isolation, embryos at 13.5 days post coitum from C57BL/6J mice (CLEA Japan, Tokyo, Japan) were used. After the removal of the head and visceral tissues, the remaining bodies were washed and dissociated. Cells were plated on dishes and incubated 37°C with 5% CO<sub>2</sub>. The next day, floating cells were removed by washing in PBS. MEFs were used within three passages. Cells and MEFs were maintained in Dulbecco's modified Eagle's medium (DMEM; Gibco™, Thermo Fisher Scientific) supplemented with 10% fetal bovine serum (FBS; Gibco™, Thermo Fisher Scientific) and penicillin–streptomycin (Sigma-Aldrich).

### Antibodies

Antibodies against the following proteins and epitopes were used in this study:  $\beta$ -actin (Sigma-Aldrich; A5316; 1:5000);  $\alpha$ -tubulin (Sigma-Aldrich; T5168; 1:5000); Histone H3 (Cell Signaling Technology; 9715; 1:3000); 1-methyladenosine (m<sup>1</sup>A; MBL International, Nagoya, Japan; D345-3); RPL11 (Cell Signaling Technology; 14382; 1:2000); MDM2 (Santa Cruz Biotechnology; sc-965; 1:500); p53 (DO-1; Santa Cruz Biotechnology; sc-126; 1:2000); 14-3-3 $\sigma$  (1.N.6; Abcam; ab14123; 1:2000); Bax (Abcam; ab7977; 1:1000); and an unconjugated affinity purified isotype control immunoglobulin (IgG) from mouse (Santa Cruz Biotechnology; sc-2025).

Previously reported anti-human and mouse NML antibodies were generated (1:1000) (Murayama et al., 2008; Oie et al., 2014).

### RNA interference

To generate stable knockdown cell lines, cells were transfected with the piGENE™ hU6 plasmid (iGENE Therapeutics, Tsukuba, Japan) containing sequences targeting NML, GFP or luciferase (Luc). The transfected cells were selected with puromycin. The target sequences were: 5'-GCCGCTT-TGAGGATGTTCGAA-3' for shNML#1; 5'-GGGTAGTACTACAAAT-GATCC-3' for shNML#2 (Murayama et al., 2008); 5'-GGCTACGTCCA-GGAGCGCACC-3' for shGFP; and 5'-GTGCGCTGCTGGTCCCAACC-C-3' for shLuc.

For transient knockdown, cells were transfected with 20 nM of Stealth RNAi™ short interfering RNA (siRNA) (Invitrogen) using Lipofectamine® RNAiMAX (Invitrogen) according to the manufacturer's protocol. The target sequences were as follows: 5'-CCGCUUUGAGGAUGUUCGAA-CCUUU-3' for siNML#1 (human); 5'-CCUCAUACAUUAAGCCGCA-AGCAGU-3' for siNML#2 (human); 5'-CCAAACUCGGCUUUAAGA-UUAUCUA-3' for siNML (mouse); 5'-ACACAUCGAUCUGGGUAUC-AAAUAU-3' for siRPL11. Stealth RNAi™ Luciferase Reporter control (siLuc) was used as a negative control.

### Plasmid construction and mutagenesis

A plasmid containing mouse wild-type NML was constructed by inserting the *HindIII*–*NotI* (blunt ended with Klenow)-digested fragment from FLAG- and HA-tagged mouse NML in pcDNA3 (a gift from Dr Murayama, University of Tsukuba, Tsukuba, Japan) into the *XhoI* (filled with Klenow) site of the plasmid pPB-CAG.EBNXN (kindly provided by Dr Allan Bradley, Wellcome Trust Sanger Institute, Hinxton, Cambridgeshire, UK). Mutations were introduced by using site-directed mutagenesis and PCR. The primer sequences were as follows (altered sequences are underlined):

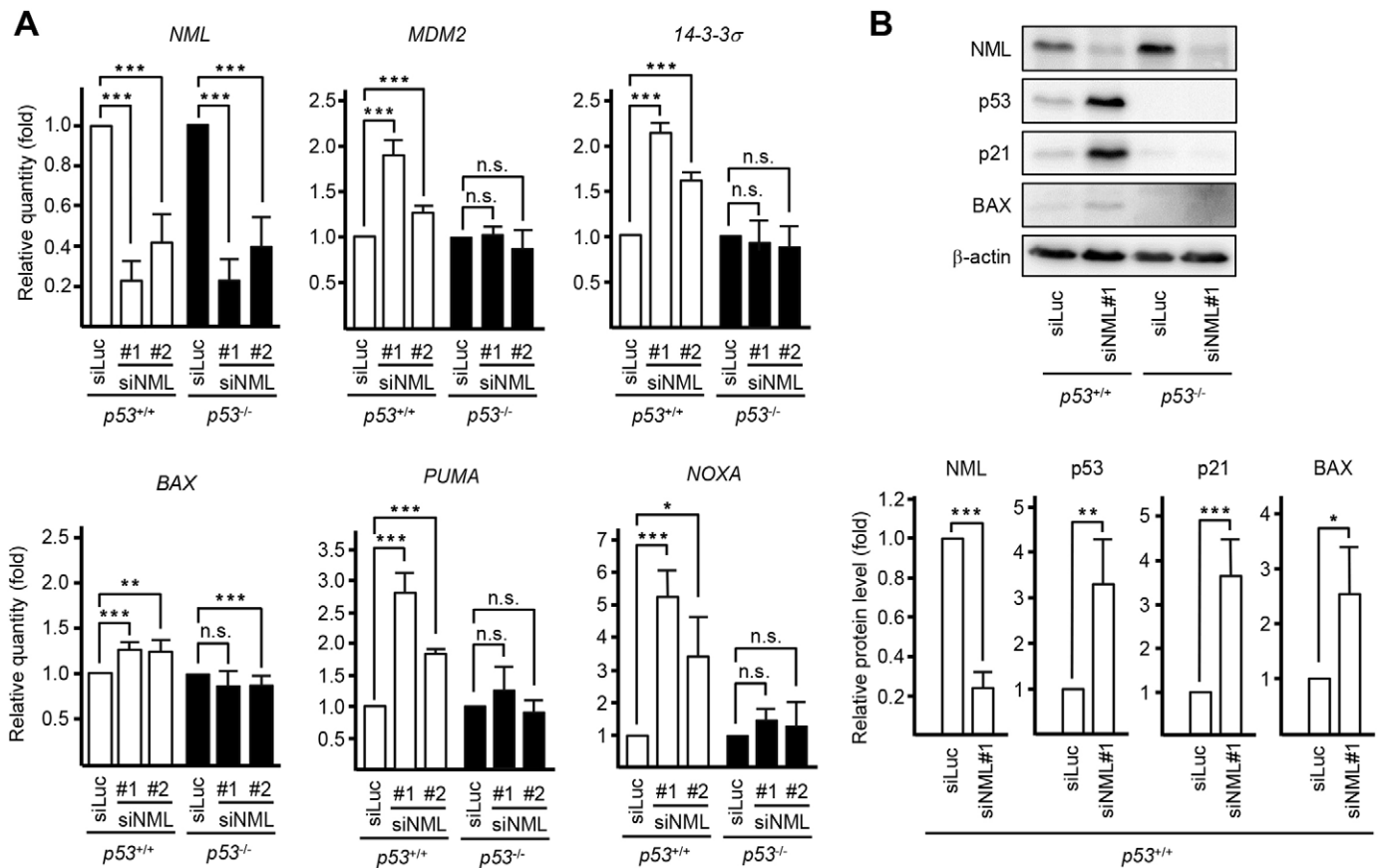


**Fig. 7. NML depletion activates the p53 pathway.** (A) mRNA levels of p53 target genes in HCT116 p53<sup>+/+</sup> or p53<sup>-/-</sup> cells that had been treated with siLuc or siNML#1 or siNML#2. Three days after siRNA transfection, the levels of the indicated mRNA were analyzed by performing qRT-PCR. Graphs are expressed as the fold change relative to corresponding mRNA levels in siLuc-transfected HCT116 p53<sup>+/+</sup> or p53<sup>-/-</sup> cells. (B) Protein levels of p53 targets in HCT116 p53<sup>+/+</sup> or p53<sup>-/-</sup> cells that had been treated with siLuc or siNML#1. Three days after siRNA transfection, the indicated protein levels were analyzed using western blot. Representative western blot data are shown in the upper panel. Graphs show the fold change relative to the indicated protein levels in siLuc-transfected HCT116 p53<sup>+/+</sup> cells (lower panel). All values are presented as mean±s.d. of three independent experiments. \**P*<0.05; \*\**P*<0.01; \*\*\**P*<0.005; n.s., not significant (bootstrap and permutation tests).

mouse NML mt1 (G317D,G319R), 5'-GCTGACTTTGACTGTAGAGATTGCCGC-3'; mouse NML mt2 (G317Q), 5'-GCTGACTTTGGCTGTGAAAGATTGCCGC-3'.

#### Western blotting

To detect proteins using western blotting, cells were lysed with RIPA buffer [20 mM Tris-HCl (pH 7.5), 150 mM NaCl, 2 mM EDTA, 0.8% Nonidet P-40 (NP-40), 0.1% sodium dodecyl sulfate (SDS) and 0.5% sodium deoxycholate]. Cell extracts were fractionated by performing SDS-PAGE and transferred to a polyvinylidene difluoride membrane using transfer apparatus according to the manufacturer's protocol (Bio-Rad Laboratories). The antibodies used are described in the Antibodies section. Quantitative analyses of western blot data were performed using Multi Gauge version 3.0 software (Fujifilm). Each protein level was normalized to the protein levels of β-actin.

#### Co-immunoprecipitation

Cells were lysed in RIPA buffer supplemented with EDTA-free protease inhibitor cocktail (Nacalai Tesque, Kyoto, Japan). Equal amounts of extracted proteins were resuspended in TNE buffer [10 mM Tris-HCl (pH 7.5), 150 mM NaCl, 1 mM EDTA, 1% NP-40] supplemented with EDTA-free protease inhibitor cocktail, and were immunoprecipitated with the indicated antibodies (1.8 μg/ml) and Dynabeads conjugated to protein G (Invitrogen). Bound proteins were then analyzed by using western blot.

#### qRT-PCR

To quantify rRNA methylation levels, we performed a site-specific rRNA methylation assay based on quantitative reverse-transcription (qRT)-PCR

(Belin et al., 2009; Marcel et al., 2013). Total RNA was extracted and purified using Sepasol-RNA I Super G (Nacalai Tesque) according to the manufacturer's instructions. Aliquots of total RNA (500 ng) were reverse transcribed using ReverTra Ace<sup>®</sup> (Toyobo, Osaka, Japan) and 1 μM of each reverse primer targeting a sequence downstream to a specific methylation site, with either a low (2.5 μM) or high (250 μM) deoxy nucleoside triphosphate (dNTP) concentration, according to the manufacturer's instructions. qRT-PCR was performed with SYBR<sup>®</sup> Premix Ex Taq<sup>™</sup> II (Takara Bio, Otsu, Japan) using a Thermal Cycler Dice<sup>™</sup> Real-Time System (Takara Bio). The amount of methylation was calculated following the function  $2^{-(CT_{low}-CT_{high})}$ , where the CT (threshold cycle) value obtained with the qRT-PCR reaction at the low dNTP concentration was normalized to that obtained at the high dNTP concentration. We used the following primer sets: hA1309\_RT and hA1309\_Fw/Rv; hA3625\_RT and hA3625\_Fw/Rv; mA1136\_RT and mA1136\_Fw/Rv; and mA3301\_RT and mA3301\_Fw/Rv (Table S1).

To quantify rRNA or mRNA levels, aliquots of total RNA (500 ng) were reverse transcribed with a pd(N)6 random primer and 250 μM of dNTPs. qRT-PCR was performed with primers for the indicated rRNA or genes (Table S1). The expression level of each gene in human and mouse cells was normalized to the mRNA levels of genes encoding human β-actin (*ACTB*) and mouse cyclophilin (*Ppia*), respectively.

#### RNA immunoprecipitation

RIP was performed as previously described (Lin et al., 2011) with minor modifications. For RIP against NML using nuclear lysates, cells were harvested and resuspended in 450 μl buffer A [10 mM HEPES (pH 7.5), 10 mM KCl, 0.1 mM EDTA] (Dignam et al., 1983) and kept on ice for

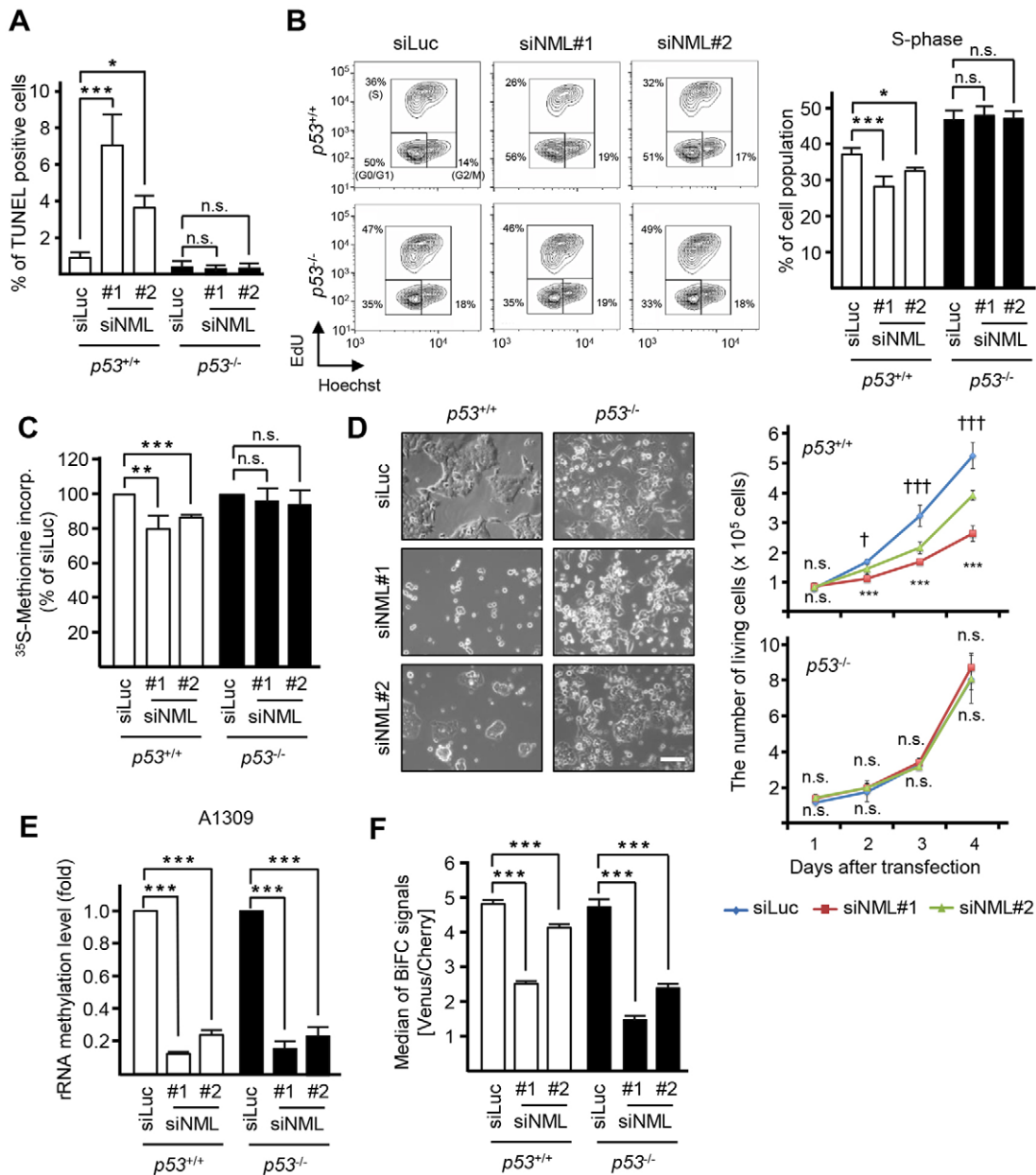


**Fig. 8. NML regulates cell proliferation in a p53-dependent manner.** (A) Apoptosis assay of HCT116  $p53^{+/+}$  or  $p53^{-/-}$  cells that had been treated with siLuc, or siNML#1 or siNML#2. Three days after siRNA transfection, the cells indicated were analyzed using TUNEL staining. For each group, cells were counted in three randomly selected fields (more than 100 cells/field) per experiment. (B) Cell cycle analysis of HCT116  $p53^{+/+}$  or  $p53^{-/-}$  cells that had been treated with siLuc, or siNML#1 or siNML#2. Three days after siRNA transfection, the indicated cells were analyzed using EdU staining following FACS analysis (left panel). The percentages of the cell population in the S-phase were compared between the indicated cells (right panel). (C) The total protein synthesis rates in the cells indicated were measured based on <sup>35</sup>S-methionine incorporation (incorp.) into newly synthesized proteins 3 days after siRNA transfection. (D) Phase-contrast images and growth curve of HCT116  $p53^{+/+}$  or  $p53^{-/-}$  cells that had been treated with siLuc, or siNML#1 or siNML#2. The phase-contrast images (left panel) were taken three days after siRNA transfection. Scale bar: 100  $\mu$ m. Living cells were counted at the times indicated after siRNA transfection using Trypan Blue staining (right panel). The statistical significance between siLuc- and siNML#1- or siNML#2-expressing cells is shown by \* and †, respectively. (E) Methylation levels at the region of 28S rRNA that includes A1309 in HCT116  $p53^{+/+}$  or  $p53^{-/-}$  cells that had been treated with the indicated siRNAs. Three days after siRNA transfection, methylation levels were analyzed by performing qRT-PCR. (F) The median BiFC signals in HCT116  $p53^{+/+}$  or  $p53^{-/-}$  cells that had been treated with the indicated siRNAs. Three days after siRNA transfection, BiFC signals were analyzed by performing FACS. All values are presented as mean  $\pm$  s.d. of three independent experiments in A–C, E, F and of three wells in D from a representative experiment that was performed at least three times with similar results. \* or †  $P < 0.05$ ; \*\*  $P < 0.01$ ; \*\*\* or †††  $P < 0.005$ ; n.s., not significant (one-way ANOVA followed by Tukey's test) in A, B, D, F. \*\*  $P < 0.01$ ; \*\*\*  $P < 0.005$ ; n.s., not significant (bootstrap and permutation tests) in C, E.

15 min. Fifty microliters of 5% NP-40 in buffer A were added. Nuclei were pelleted by centrifugation at 800  $g$  for 5 min. Then, whole cells or nuclei were suspended in 200  $\mu$ l cold lysis buffer [10 mM 4-(2-hydroxyethyl)-1-piperazineethanesulfonic acid (pH 7.5), 300 mM KCl, 5 mM MgCl<sub>2</sub>, 0.5% NP-40, 1 mM dithiothreitol, EDTA-free protease inhibitor cocktail (Nacalai

Tesque) and 100 U/ml RNase Inhibitor (Toyobo)]. Whole-cell or nuclear extracts were centrifuged at 15,000  $g$  for 15 min at 4°C, and the supernatant was pre-cleared using protein-G-Sepharose® beads (GE Healthcare) and treated with DNase I (Wako Pure Chemical Industries, Osaka, Japan) (60 U/100  $\mu$ l lysate) for 30 min on ice. The samples (2–10  $\mu$ g) were incubated with

pre-binding antibodies (5 µg) and protein-G–Sepharose® beads in 1000 µl NT2 buffer [50 mM Tris-HCl (pH 7.5), 150 mM NaCl, 1 mM MgCl<sub>2</sub> and 0.05% NP-40] including 100 U of RNase inhibitor, 10 mM dithiothreitol and 20 mM EDTA overnight at 4°C. The beads were washed twice with NT2 buffer and resuspended in 100 µl of NT2 buffer. The suspension was mixed with 100 µl of proteinase K buffer [30 µg proteinase K, 20 mM Tris-HCl (pH 7.8), 10 mM EDTA and 1.0% SDS] and incubated for 30 min at 55°C. After centrifugation, RNAs were purified from the supernatant using phenol–chloroform–isoamyl-alcohol and analyzed by performing qRT-PCR. Whole-cell or nuclear extracts were used as input samples for normalization of qRT-PCR data.

For RIP against m<sup>1</sup>A, total RNAs were extracted using Sepazol-RNA I Super G and treated with DNase I. Purified RNAs were fragmented using an NEBNext® Magnesium RNA Fragmentation Module (New England Biolabs). Fragmented RNAs were precipitated with ethanol after adding 20 µg of glycogen and resuspended in 100 µl of IPP buffer [10 mM Tris-HCl (pH 7.5), 150 mM NaCl and 0.1% NP-40]. RNA samples were added to 100 µl of an antibody mixture that included IPP buffer and 50 µl of protein-G–Sepharose® beads. The mixture was rotated overnight at 4°C. The beads were washed twice with IPP buffer. Immunoprecipitated RNAs were purified by phenol–chloroform–isoamyl-alcohol extraction, and analyzed using qRT-PCR. Total RNAs were used as input samples for normalization of qRT-PCR data.

### Primer extension

Primer extension was performed as per previously described protocols (Cozen et al., 2015; Sharma et al., 2013) with minor modifications. One micromole of DNA primer was <sup>32</sup>P-5'-terminally labeled by incubation in a final volume of 25 µl with 15 µCi γ-[<sup>32</sup>P]ATP and 9 U of polynucleotide kinase in protruding kinase buffer (Toyobo). The reaction was incubated at 37°C for 1 h. The reaction mixture was then purified using Illustra™ MicroSpin™ G-25 columns (GE Healthcare). For the extension reaction, 0.5 µl of the <sup>32</sup>P-5'-phosphorylated primer was annealed by heating for 3 min at 95°C, followed by cooling on ice using 0.2 µg total RNA in 4.75 µl RT buffer (Toyobo) containing 2.5 µM dNTPs. Annealed primers were extended using 0.25 µl ReverTra Ace® (25 U) for 1 h at 42°C, stopped by the addition of 5 µl formamide loading dye and frozen at –80°C. Primer extension products were resolved by performing electrophoresis on 8% polyacrylamide gels containing 4 M urea. Gels were dried and exposed to Amersham Hyperfilm™ ECL (GE Healthcare). DNA primer sequences (hA1309\_RT and mA1136\_RT) used for primer extension are listed in Table S1.

### Quantification of methylated ribonucleosides with LC-MS/MS

28S rRNA was isolated from total RNA by performing agarose gel electrophoresis and using the NucleoSpin® Gel and PCR Clean-up system (Macherey-Nagel, Düren, Germany) according to the instruction manual. After denaturation by heating at 100°C for 3 min, 1–2 µg of 28S rRNA was immediately chilled on ice. Denatured RNA was hydrolyzed by 1 U of nuclease P1 (Wako Pure Chemical Industries) in 10 mM ammonium acetate buffer (pH 5.3) at 45°C for 2 h, subsequently dephosphorylated by incubating with phosphodiesterase I (0.0002 U, Sigma-Aldrich), alkaline phosphatase (0.3 U, Toyobo) and 0.1 volume of 1 M ammonium bicarbonate buffer (pH 7.9) at 37°C for 2 h, as described previously (Crain, 1990). Ten pmol of br<sup>5</sup>U (Tokyo Chemical Industry, Tokyo, Japan) were added into the digestion mixture as an internal standard; the enzymes were subsequently removed by acetone precipitation. The supernatant was left to evaporate, and the ribonucleoside powder was dissolved with 15 µl of HPLC-grade water (Wako Pure Chemical Industries).

Individual ribonucleosides were quantified using a Shimadzu Nexera™ UHPLC system coupled to LCMS-8050™ triple quadrupole mass spectrometer (Shimadzu, Kyoto, Japan). Reverse-phase HPLC separation was carried out using a Kinetex™ 2.6 µm C18 column (2.1×150 mm, Phenomenex, Torrance, CA, USA) with a VANGUARD™ Pre-Column (2.1×5 mm, Waters Co., Milford, MA, USA) at 30°C with 80% acetonitrile in 0.1% formic acid (solvent B) gradient in 0.1% formic acid (solvent A) at a flow rate of 0.2 ml/min. The abovementioned water-dissolved sample (5 µl) was injected and eluted with the following gradient elution: initial isocratic

elution with 0% solvent B for 3 min, followed by linear gradient elution from 0 to 8% B until 19 min, jumping to 100% B within 2 min and holding the status until 25.5 min. The column was then subsequently returned to the initial conditions within 1 min and equilibrated for 4.5 min before the next sample injection. For determining elution positions of ribonucleosides on the chromatogram, standard chemicals of m<sup>1</sup>A (Santa Cruz Biotechnology), N<sup>6</sup>-methyladenosine (m<sup>6</sup>A) (Carbosynth, Compton, Berkshire, UK) and br<sup>5</sup>U were used, and their retention times were revealed as 2.23 min, 15.1 min and 11.58 min, respectively.

The mass spectrometer was operated with an ion-spray source at 300°C in positive ion mode, with unit resolution for Q1 and Q3, and other optimized parameters: interface voltage, 4.0 kV; interface current, 0.1 µA; flow rate of nebulizer gas, 3 l/min; flow rate of heating gas, 10 l/min; flow rate of drying gas, 10 l/min; collision gas (Ar), 270 kPa; desolvation line temperature, 250°C; heat block temperature, 400°C; conversion dynode potential, 10 kV; detector potential, 2.44 kV. Multiple reaction monitoring was used for detection of nucleosides with a dwell time of up to 100 ms. Q1 was set to transmit the parental ions MH<sup>+</sup> at *m/z* 282.1, 282.1 and 324.6 for m<sup>1</sup>A, m<sup>6</sup>A and br<sup>5</sup>U, respectively. The daughter ions were monitored in Q3 at *m/z* 150.1, 150.1 and 193.05 for m<sup>1</sup>A, m<sup>6</sup>A and br<sup>5</sup>U, respectively. Linear calibration curves were obtained daily.

All of the solvents and reagents used in this analysis were HPLC grade. Instrument control and data processing were performed using the LabSolutions LCMS (Ver.5.60) software (Shimadzu Co.).

### Bimolecular fluorescence complementation

The BiFC assay was performed as described previously (Al-Jubran et al., 2013). To generate plasmids expressing BiFC-tagged ribosomal proteins, the sequences of *RPS18* and *RPL11* were PCR-amplified from the cDNA of HeLa cells using primers tagged with *SacI* and *XbaI* or *ApaI* and *KpnI*, respectively. *RPS18* and *RPL11* segments were cloned into pBiFC-VN173 (Addgene, 22010) and pBiFC-VC155 (Addgene, 22011), respectively (Shyu et al., 2008). Using Lipofectamine® LTX (Invitrogen), these BiFC plasmids were co-transfected with a pmCherry-N1 plasmid (Clontech Laboratories), which was used as an internal control. Twenty-four hours after transfection, cells were further cultured with or without 100 µg/ml puromycin for 24 h. The cells were washed twice with STM buffer [phosphate-buffered saline (PBS) with 2% FBS] and resuspended in 500 µl of STM buffer. The fluorescence intensities of Venus and mCherry were measured by flow cytometry using a BD FACSAria™ II (BD Biosciences). The BiFC signal emitted by a cell was calculated using the following function: (fluorescent intensity of Venus)/(fluorescent intensity of mCherry), as previously described (Hu et al., 2002).

### rRNA processing

Cells were cultured with methionine-free medium for 1 h, and then with methionine-free medium containing 20 µCi/ml <sup>32</sup>P-labeled inorganic phosphate for 1 h (Sloan et al., 2013). The metabolic labeling media were removed, and the cells were cultured with normal medium for 3 h. RNA was extracted using a FastPure™ RNA Kit (Takara Bio) and analyzed by glyoxal agarose gel electrophoresis. Total RNA was visualized using ethidium bromide staining. The intensity of each band was analyzed with the Multi Gauge version 3.0 (Fujifilm).

### Sucrose density gradient centrifugation

Sucrose density gradient centrifugation was performed as described previously (Peifer et al., 2013; Tuorto et al., 2012).

To investigate ribosomal subunit formation, cells were treated with 100 µg/ml cycloheximide (CHX) in culture medium for 5 min at 37°C. The cells were washed twice with PBS containing CHX (100 µg/ml) and lysed with lysis buffer [15 mM Tris-HCl (pH 7.5), 300 mM NaCl, 25 mM EDTA, 1% Triton X-100, 0.5 mg/ml heparin, 100 µg/ml CHX, 1× EDTA-free protease inhibitor cocktail (Nacalai Tesque) and 100 U/ml RNase inhibitor (Toyobo)]. The lysate was centrifuged at 9300 *g* for 10 min at 4°C and loaded onto a linear 20–50% sucrose gradient buffer in 15 mM Tris-HCl (pH 8.0), 25 mM EDTA and 300 mM NaCl. Centrifugation was conducted at 40,000 rpm for 2 h at 4°C in a SW-41 Ti rotor (Beckman Coulter), and

fractions were collected from the top of the gradient (#1 to #19). The 18S and 28S rRNA levels in the fractions #1 to #18 were quantified by performing qRT-PCR and normalized against those rRNA levels in an input control. The ratio of 18S rRNA:28S rRNA (18S rRNA divided by 28S rRNA) was calculated as the small:large ribosomal subunit ratio.

To obtain the ribosomal or ribosome-free fractions, we performed sucrose density gradient centrifugation using lysis and gradient buffers containing 15 mM MgCl<sub>2</sub> instead of 25 mM EDTA. 18S and 28S rRNAs, and β-actin proteins were used as indicators for the ribosomal and ribosome-free fractions, respectively (Lee et al., 2013; Morello et al., 2011).

### Analysis of protein synthesis using <sup>35</sup>S-methionine incorporation

This experiment was performed as previously described (Itani et al., 2003; Mieulet et al., 2007). Cells were plated onto 12-well plates in complete medium and transfected with or without siRNAs. One day after cell seeding or 3 days after transfection, the culture medium was switched to methionine-free DMEM with or without 50 μg/ml CHX for 30 min at 37°C, and cells were incubated with the same medium containing 20 μCi/ml <sup>35</sup>S-methionine (PerkinElmer) for 2 h at 37°C. Cells were then washed twice with ice-cold PBS and solubilized in 50 μl of RIPA buffer containing protease inhibitors. Aliquots of the supernatant were analyzed using a liquid scintillation counter (Beckman Coulter) and normalized against the total protein content.

### 5-ethynyl-2'-deoxyuridine staining for cell cycle analysis

For 5-ethynyl-2'-deoxyuridine (EdU) staining, cells were plated (1×10<sup>5</sup> cells/well in a 6-well plate) and cultured for the indicated number of days after siRNA transfection. Then, this experiment was conducted using a Click-iT<sup>®</sup> EdU Imaging Kit (Invitrogen), according to the manufacturer's protocol. First, cells were labeled with 10 μM EdU (Invitrogen) in culture medium for 1 h at 37°C. For subsequent DNA staining, EdU-stained cells were incubated with 2 μg/ml Hoechst 33342 (Sigma-Aldrich) for 10 min. Then the cells were washed with PBS and subjected to FACS by using flow cytometry in a BD FACSAria<sup>™</sup> II instrument (BD Biosciences).

### Terminal deoxynucleotidyl transferase dUTP nick-end labeling assay

Cells were plated onto poly-D-lysine-coated (BD Biosciences) 8-well chamber slides (1.6×10<sup>4</sup>–2.4×10<sup>4</sup> cells/well) and cultured for 1, 2, 3 or 4 days after siRNA transfection. Then, the cells were fixed with 4% paraformaldehyde in PBS for 25 min at 4°C, and *in situ* detection of apoptotic cells was performed using DeadEnd<sup>™</sup> Fluorometric TUNEL System (Promega), according to the manufacturer's instructions. Nuclei were then counterstained using 2 μg/ml Hoechst 33342. The cells were examined using the fluorescent microscope imaging system Biorevo BZ-9000 (Keyence, Osaka, Japan), and TUNEL-positive cells were quantified in three fields per sample. The percentage of TUNEL-positive cells was calculated as follows: (TUNEL-positive/total cells)×100.

### Cell proliferation assay

We seeded 1×10<sup>5</sup> cells/well in 6-well plates and transfected them with the indicated siRNA. The cells were then trypsinized into single-cell suspensions and automatically counted using a TC10<sup>™</sup> Automated Cell Counter (Bio-Rad Laboratories) on days 1, 2, 3 and 4, where the first day after seeding was day 0.

### Statistics

The unpaired Student's *t*-test was used to compare two groups, and one-way ANOVA followed by Tukey's post-hoc test was used to compare multiple groups. The statistical analysis of fold-change data was performed by bootstrap and permutation tests using the web application Bootstratio (Clères et al., 2012).

### Acknowledgements

We are thankful to Dr Shin-ichi Kashiwabara (University of Tsukuba, Tsukuba, Japan) for his technical advice of sucrose density gradient centrifugation and primer extension assay. We are also grateful to the members of Shimizu and Fukamizu laboratories for technical advice and useful discussion.

### Competing interests

The authors declare no competing or financial interests.

### Author contributions

T.W., Y.N., W.Y. and N.N. designed and performed the experiment. T.W. and Y.N. wrote the manuscript. K.K., A.K., T.S. and A.F. supervised the project and helped prepare the manuscript.

### Funding

This work was supported by Grant-in-Aid for Scientific Research on Innovative Areas (Japan Society for the Promotion of Science) [grant numbers 26116725 to A.K., 23116007 to T.S. and 23116004 to A.F.]; and the Open Innovation Core (OIC) Project (Y.N.; a member of OIC) of Life Science Center, Tsukuba Advanced Research Alliance, University of Tsukuba, Japan.

### Supplementary information

Supplementary information available online at <http://jcs.biologists.org/lookup/doi/10.1242/jcs.183723.supplemental>

### References

- Al-Jubran, K., Wen, J., Abdullahi, A., Roy Chaudhury, S., Li, M., Ramanathan, P., Matina, A., De, S., Piechocki, K., Rugjee, K. N. et al. (2013). Visualization of the joining of ribosomal subunits reveals the presence of 80S ribosomes in the nucleus. *RNA* **19**, 1669–1683.
- Anger, A. M., Armache, J.-P., Berninghausen, O., Habeck, M., Subklewe, M., Wilson, D. N. and Beckmann, R. (2013). Structures of the human and Drosophila 80S ribosome. *Nature* **497**, 80–85.
- Barna, M., Pusic, A., Zollo, O., Costa, M., Kondrashov, N., Rego, E., Rao, P. H. and Ruggero, D. (2008). Suppression of Myc oncogenic activity by ribosomal protein haploinsufficiency. *Nature* **456**, 971–975.
- Belin, S., Beghin, A., Solano-Gonzalez, E., Bezin, L., Brunet-Manquat, S., Textoris, J., Prats, A.-C., Mertani, H. C., Dumontet, C. and Diaz, J.-J. (2009). Dysregulation of ribosome biogenesis and translational capacity is associated with tumor progression of human breast cancer cells. *PLoS ONE* **4**, e7147.
- Belin, S., Kindbeiter, K., Hacot, S., Albaret, M. A., Roca-Martinez, J.-X., Therizols, G., Grosso, O. and Diaz, J.-J. (2010). Uncoupling ribosome biogenesis regulation from RNA polymerase I activity during herpes simplex virus type 1 infection. *RNA* **16**, 131–140.
- Biegging, K. T., Mello, S. S. and Attardi, L. D. (2014). Unravelling mechanisms of p53-mediated tumour suppression. *Nat. Rev. Cancer* **14**, 359–370.
- Blobel, G. and Sabatini, D. (1971). Dissociation of mammalian polyribosomes into subunits by puromycin. *Proc. Natl. Acad. Sci. USA* **68**, 390–394.
- Bousquet-Antonelli, C., Vanrobays, E., Gelugne, J.-P., Caizergues-Ferrer, M. and Henry, Y. (2000). Rrp8p is a yeast nucleolar protein functionally linked to Gar1p and involved in pre-rRNA cleavage at site A2. *RNA* **6**, 826–843.
- Brooks, C. L. and Gu, W. (2010). New insights into p53 activation. *Cell Res.* **20**, 614–621.
- Bunz, F., Dutriaux, A., Lengauer, C., Waldman, T., Zhou, S., Brown, J. P., Sedivy, J. M., Kinzler, K. W. and Vogelstein, B. (1998). Requirement for p53 and p21 to sustain G2 arrest after DNA damage. *Science* **282**, 1497–1501.
- Clères, R., Galvez, J., Espino, M., Ribes, J., Nunes, V. and de Heredia, M. L. (2012). Bootstratio: a web-based statistical analysis of fold-change in qPCR and RT-qPCR data using resampling methods. *Comput. Biol. Med.* **42**, 438–445.
- Cozen, A. E., Quartley, E., Holmes, A. D., Hrabeta-Robinson, E., Phizicky, E. M. and Lowe, T. M. (2015). ARM-seq: AlkB-facilitated RNA methylation sequencing reveals a complex landscape of modified tRNA fragments. *Nat. Methods* **12**, 879–884.
- Crain, P. F. (1990). Preparation and enzymatic hydrolysis of DNA and RNA for mass spectrometry. *Methods Enzymol.* **193**, 782–790.
- Decatur, W. A. and Fournier, M. J. (2002). rRNA modifications and ribosome function. *Trends Biochem. Sci.* **27**, 344–351.
- Decatur, W. A. and Fournier, M. J. (2003). RNA-guided nucleotide modification of ribosomal and other RNAs. *J. Biol. Chem.* **278**, 695–698.
- Deisenroth, C. and Zhang, Y. (2010). Ribosome biogenesis surveillance: probing the ribosomal protein-Mdm2-p53 pathway. *Oncogene* **29**, 4253–4260.
- Dignam, J. D., Lebovitz, R. M. and Roeder, R. G. (1983). Accurate transcription initiation by RNA polymerase II in a soluble extract from isolated mammalian nuclei. *Nucleic Acids Res.* **11**, 1475–1489.
- Figueiredo, V. C., Caldow, M. K., Massie, V., Markworth, J. F., Cameron-Smith, D. and Blazeovich, A. J. (2015). Ribosome biogenesis adaptation in resistance training-induced human skeletal muscle hypertrophy. *Am. J. Physiol. Endocrinol. Metab.* **309**, E72–E83.
- Fumagalli, S., Di Cara, A., Neb-Gulati, A., Natt, F., Schwemberger, S., Hall, J., Babcock, G. F., Bernardi, R., Pandolfi, P. P. and Thomas, G. (2009). Absence of nucleolar disruption after impairment of 40S ribosome biogenesis reveals an rpL11-translation-dependent mechanism of p53 induction. *Nat. Cell Biol.* **11**, 501–508.

- Gigovas, A., Duggimpudi, S., Pollex, T., Schaefer, M. and Koš, M. (2014). A cluster of methylations in the domain IV of 25S rRNA is required for ribosome stability. *RNA* **20**, 1632–1644.
- Grummt, I. and Ladurner, A. G. (2008). A metabolic throttle regulates the epigenetic state of rDNA. *Cell* **133**, 577–580.
- Haag, S., Kretschmer, J. and Bohnsack, M. T. (2015). WBSCR22/Merm1 is required for late nuclear pre-ribosomal RNA processing and mediates N7-methylation of G1639 in human 18S rRNA. *RNA* **21**, 180–187.
- Hauenschild, R., Tserovski, L., Schmid, K., Thuring, K., Winz, M.-L., Sharma, S., Entian, K.-D., Wacheul, L., Lafontaine, D. L. J., Anderson, J. et al. (2015). The reverse transcription signature of N-1-methyladenosine in RNA-Seq is sequence dependent. *Nucleic Acids Res.* **43**, 9950–9964.
- Henras, A. K., Plisson-Chastang, C., O'Donohue, M.-F., Chakraborty, A. and Gleizes, P.-E. (2015). An overview of pre-ribosomal RNA processing in eukaryotes. *Wiley Interdiscip. Rev. RNA* **6**, 225–242.
- Hoppe-Seyler, F. and Butz, K. (1993). Repression of endogenous p53 transactivation function in HeLa cervical carcinoma cells by human papillomavirus type 16 E6, human mdm-2, and mutant p53. *J. Virol.* **67**, 3111–3117.
- Hu, C.-D., Chinenov, Y. and Kerppola, T. K. (2002). Visualization of interactions among bZIP and Rel family proteins in living cells using bimolecular fluorescence complementation. *Mol. Cell* **9**, 789–798.
- Ishitani, R., Yokoyama, S. and Nureki, O. (2008). Structure, dynamics, and function of RNA modification enzymes. *Curr. Opin. Struct. Biol.* **18**, 330–339.
- Itani, O. A., Cornish, K. L., Liu, K. Z. and Thomas, C. P. (2003). Cycloheximide increases glucocorticoid-stimulated alpha-ENaC mRNA in collecting duct cells by p38 MAPK-dependent pathway. *Am. J. Physiol. Renal Physiol.* **284**, F778–F787.
- Itoh, K., Mizugaki, M. and Ishida, N. (1988). Preparation of a monoclonal antibody specific for 1-methyladenosine and its application for the detection of elevated levels of 1-methyladenosine in urines from cancer patients. *Jpn. J. Cancer Res.* **79**, 1130–1138.
- Itoh, K., Ishiwata, S., Ishida, N. and Mizugaki, M. (1992). Diagnostic use of anti-modified nucleoside monoclonal antibody. *Tohoku J. Exp. Med.* **168**, 329–331.
- Khatter, H., Myasnikov, A. G., Natchiar, S. K. and Klaholz, B. P. (2015). Structure of the human 80S ribosome. *Nature* **520**, 640–645.
- Kierstead, T. D. and Tevethia, M. J. (1993). Association of p53 binding and immortalization of primary C57BL/6 mouse embryo fibroblasts by using simian virus 40 T-antigen mutants bearing internal overlapping deletion mutations. *J. Virol.* **67**, 1817–1829.
- Lee, M. S., Kim, B., Oh, G. T. and Kim, Y.-J. (2013). OASL1 inhibits translation of the type I interferon-regulating transcription factor IRF7. *Nat. Immunol.* **14**, 346–355.
- Lin, J., Lai, S., Jia, R., Xu, A., Zhang, L., Lu, J. and Ye, K. (2011). Structural basis for site-specific ribose methylation by box C/D RNA protein complexes. *Nature* **469**, 559–563.
- Lohrum, M. A. E., Ludwig, R. L., Kubbutat, M. H. G., Hanlon, M. and Vousden, K. H. (2003). Regulation of HDM2 activity by the ribosomal protein L11. *Cancer Cell* **3**, 577–587.
- Marcel, V., Ghayad, S. E., Belin, S., Therizols, G., Morel, A.-P., Solano-Gonzalez, E., Vendrell, J. A., Hacot, S., Mertani, H. C., Albaret, M. A. et al. (2013). p53 acts as a safeguard of translational control by regulating fibrillarin and rRNA methylation in cancer. *Cancer Cell* **24**, 318–330.
- Mieulet, V., Roceri, M., Espeillac, C., Sotiropoulos, A., Ohanna, M., Oorschot, V., Klumperman, J., Sandri, M. and Pende, M. (2007). S6 kinase inactivation impairs growth and translational target phosphorylation in muscle cells maintaining proper regulation of protein turnover. *Am. J. Physiol. Cell Physiol.* **293**, C712–C722.
- Miliani de Marval, P. L. and Zhang, Y. (2011). The RP-Mdm2-p53 pathway and tumorigenesis. *Oncotarget* **2**, 234–238.
- Morello, L. G., Hesling, C., Coltri, P. P., Castilho, B. A., Rimokh, R. and Zanchin, N. I. T. (2011). The NIP7 protein is required for accurate pre-rRNA processing in human cells. *Nucleic Acids Res.* **39**, 648–665.
- Murayama, A., Ohmori, K., Fujimura, A., Minami, H., Yasuzawa-Tanaka, K., Kuroda, T., Oie, S., Daitoku, H., Okuwaki, M., Nagata, K. et al. (2008). Epigenetic control of rDNA loci in response to intracellular energy status. *Cell* **133**, 627–639.
- Nissen, P., Hansen, J., Ban, N., Moore, P. B. and Steitz, T. A. (2000). The structural basis of ribosome activity in peptide bond synthesis. *Science* **289**, 920–930.
- Oie, S., Matsuzaki, K., Yokoyama, W., Tokunaga, S., Waku, T., Han, S.-I., Iwasaki, N., Mikogai, A., Yasuzawa-Tanaka, K., Kishimoto, H. et al. (2014). Hepatic rRNA transcription regulates high-fat-diet-induced obesity. *Cell Rep.* **7**, 807–820.
- Peifer, C., Sharma, S., Watzinger, P., Lamberth, S., Kotter, P. and Entian, K.-D. (2013). Yeast Rrp8p, a novel methyltransferase responsible for m1A 645 base modification of 25S rRNA. *Nucleic Acids Res.* **41**, 1151–1163.
- Polikanov, Y. S., Melnikov, S. V., Söll, D. and Steitz, T. A. (2015). Structural insights into the role of rRNA modifications in protein synthesis and ribosome assembly. *Nat. Struct. Mol. Biol.* **22**, 342–344.
- Schösserer, M., Minois, N., Angerer, T. B., Amring, M., Dellago, H., Harreither, E., Calle-Perez, A., Pircher, A., Gerstl, M. P., Pfeifenberger, S. et al. (2015). Methylation of ribosomal RNA by NSUN5 is a conserved mechanism modulating organismal lifespan. *Nat. Commun.* **6**, 6158.
- Sharma, S. and Lafontaine, D. L. J. (2015). 'View From A Bridge': a new perspective on eukaryotic rRNA base modification. *Trends Biochem. Sci.* **40**, 560–575.
- Sharma, S., Watzinger, P., Kotter, P. and Entian, K.-D. (2013). Identification of a novel methyltransferase, Bmt2, responsible for the N-1-methyl-adenosine base modification of 25S rRNA in *Saccharomyces cerevisiae*. *Nucleic Acids Res.* **41**, 5428–5443.
- Shyu, Y. J., Suarez, C. D. and Hu, C.-D. (2008). Visualization of ternary complexes in living cells by using a BiFC-based FRET assay. *Nat. Protoc.* **3**, 1693–1702.
- Sloan, K. E., Bohnsack, M. T. and Watkins, N. J. (2013). The 5S RNP couples p53 homeostasis to ribosome biogenesis and nucleolar stress. *Cell Rep.* **5**, 237–247.
- Steitz, T. A. and Moore, P. B. (2003). RNA, the first macromolecular catalyst: the ribosome is a ribozyme. *Trends Biochem. Sci.* **28**, 411–418.
- Sulic, S., Panic, L., Barkic, M., Mercep, M., Uzelac, M. and Volarevic, S. (2005). Inactivation of S6 ribosomal protein gene in T lymphocytes activates a p53-dependent checkpoint response. *Genes Dev.* **19**, 3070–3082.
- Tilleray, V., Constantinou, C. and Clemens, M. J. (2006). Regulation of protein synthesis by inducible wild-type p53 in human lung carcinoma cells. *FEBS Lett.* **580**, 1766–1770.
- Tuorto, F., Liebers, R., Musch, T., Schaefer, M., Hofmann, S., Kellner, S., Frye, M., Helm, M., Stoeklin, G. and Lyko, F. (2012). RNA cytosine methylation by Dnmt2 and NSun2 promotes tRNA stability and protein synthesis. *Nat. Struct. Mol. Biol.* **19**, 900–905.
- Vousden, K. H. (2000). p53: death star. *Cell* **103**, 691–694.
- White, J., Li, Z., Sardana, R., Bujnicki, J. M., Marcotte, E. M. and Johnson, A. W. (2008). Bud23 methylates G1575 of 18S rRNA and is required for efficient nuclear export of pre-40S subunits. *Mol. Cell Biol.* **28**, 3151–3161.
- Yang, L., Song, T., Chen, L., Kabra, N., Zheng, H., Koomen, J., Seto, E. and Chen, J. (2013). Regulation of SirT1-nucleomethylin binding by rRNA coordinates ribosome biogenesis with nutrient availability. *Mol. Cell Biol.* **33**, 3835–3848.
- Zhang, Y. and Lu, H. (2009). Signaling to p53: ribosomal proteins find their way. *Cancer Cell* **16**, 369–377.
- Zhang, Y., Wolf, G. W., Bhat, K., Jin, A., Allio, T., Burkhart, W. A. and Xiong, Y. (2003). Ribosomal protein L11 negatively regulates oncoprotein MDM2 and mediates a p53-dependent ribosomal-stress checkpoint pathway. *Mol. Cell Biol.* **23**, 8902–8912.